Atmospheric Environment 45 (2011) 6241–6250

Contents lists available at ScienceDirect

Atmospheric Environment

journal homepage: www.elsevier.com/locate/atmosenv

Application of WRF/Chem-MADRID for real-time air quality forecasting over the Southeastern United States

Ming-Tung Chuang [a], Yang Zhang [a,*], Daiwen Kang [b]

[a] Air Quality Forecasting Lab, North Carolina State University, Raleigh, NC 27695, USA
[b] Computer Science Corporation, Research Triangle Park, NC 27709, USA

ARTICLE INFO

Article history:
Received 3 March 2011
Received in revised form
22 June 2011
Accepted 24 June 2011

Keywords:
O_3
$PM_{2.5}$
WRF/Chem-MADRID
Online-coupled model
Discrete evaluation
Categorical evaluation

ABSTRACT

A Real-Time Air Quality Forecast (RT-AQF) system that is based on a three-dimensional air quality model provides a powerful tool to forecast air quality and advise the public with proper preventive actions. In this work, a new RT-AQF system is developed based on the online-coupled Weather Research and Forecasting model with Chemistry (WRF/Chem) with the Model of Aerosol Dynamics, Reaction, Ionization, and Dissolution (MADRID) (referred to as WRF/Chem-MADRID) and deployed in the southeastern U.S. during May–September, 2009. Max 1-h and 8-h average ozone (O_3) and 24-h average fine particulate matter ($PM_{2.5}$) are evaluated against surface observations from the AIRNow database in terms of spatial distribution, temporal variation, and domain-wide and region-specific discrete and categorical performance statistics. WRF/Chem-MADRID demonstrates good forecasting skill that is consistent with current RT-AQF models. The overpredictions of O_3 and underprediction of $PM_{2.5}$ are likely due to uncertainties in emissions such as those of biogenic volatile organic compounds (BVOCs) and ammonia, inaccuracies in simulated meteorological variables such as 2-m temperature, 10-m wind speed, and precipitation, and uncertainties in the boundary conditions. Sensitivity simulations show that the use of the online BVOC emissions can improve $PM_{2.5}$ forecast in areas with high BVOC emissions and adjusting lateral boundaries can improve domain-wide O_3 and $PM_{2.5}$ predictions. Several limitations and uncertainties are identified to further improve the model's forecasting skill.

1. Introduction

Air quality is related to human health, crops growth, and ecological system (e.g., Utell, 2006; Krupa et al., 2006). Approximately 127 million people in the U.S. were exposed to unhealthy levels of certain air pollutants in 2008 (http://www.epa.gov/airtrends/aqtrends.html). It is important to forecast air quality and provide this information to the public in advance. This information can be valuable to susceptible subpopulations (e.g., children, the elderly, and the asthmatics). Additionally, it can help government agencies to take preventive steps such as temporarily shutting off major emission sources to alleviate air pollution. Real-time air quality forecasting (RT-AQF) has become a common practice in recent years for many local and state air quality management agencies (McHenry et al., 2004; Otte et al., 2005). At present, daily RT-AQF is issued in more than 300 cities in 50 states by local, state, and federal agencies in the U.S. and many other cities in more than 37 countries around the world (http://www.airnow.gov).

Existing AQF tools include simple rules of thumb in which thresholds of forecasted meteorological variables can indicate future high pollutant concentrations based on their correlation derived from observed and forecasted meteorological and air quality data, statistical methods in which different functions (e.g., regression or trained neural network systems) are used to forecast pollutant concentrations, and chemical transport models (CTMs) in which major atmospheric processes that affect air pollutants are simulated. Among these tools, statistical methods have been widely used due to their computational efficiency and some forecasting skill (e.g., Cobourn, 2007). CTMs for RT-AQF, despite their computational expenses, provide direct linkages between ambient precursor emissions and resultant pollution and the interrelationships among multiple pollutants (e.g., Cai et al., 2008; Mathur et al., 2008; Yu et al., 2008). Neither of them can be treated based on first principal using other types of AQF tools. The use of CTMs for AQF represents a significant advancement in routine operational RT-AQF and would greatly enhance understanding of the underlying

* Corresponding author. Air Quality Forecasting Lab, North Carolina State University, Campus Box 8208, Room 5151, Jordan Hall, 2800 Faucette Drive, Raleigh, NC 27695-8208, USA. Tel.: +1 919 515 9688; fax: +1 919 515 7802.
E-mail address: yang_zhang@ncsu.edu (Y. Zhang).

1352-2310/$ – see front matter © 2011 Elsevier Ltd. All rights reserved.
doi:10.1016/j.atmosenv.2011.06.071

complex interplay of meteorology, emissions, and chemistry. Recent AQF evaluation demonstrates that CTMs have skill consistent with or in some cases better than current statistical forecast tools (McHenry et al., 2004; Otte et al., 2005; Eder et al., 2006; Cai et al., 2008; Chen et al., 2008; Yu et al., 2008; Mathur et al., 2008).

The majority of RT-AQF with CTMs uses offline-coupled meteorology and air quality models (e.g., Cai et al., 2008; Chen et al., 2008; Yu et al., 2008; Gualtieri, 2010). These models do not permit the simulation of meteorology-chemistry feedbacks such as aerosol feedbacks to radiation, photolysis, and meteorology, which affect the next hour's air quality and meteorological predictions (Zhang, 2008; Zhang et al., 2010a,b). Fewer studies have used online-coupled meteorology-chemistry models (e.g., Grell et al., 2005; McKeen et al., 2005, 2007; Flemming et al., 2009). The use of offline-coupled systems may introduce biases in AQF. For example, Otte et al. (2005) and Eder et al. (2006) reported a poor performance of the Eta/Community Multiscale Air Quality model system (CMAQ) modeling system during cloudy periods due to the neglect of aerosol feedbacks to radiation and cloud formation processes. Furthermore, atmospheric information at a time scale smaller than the output time interval of the meteorological model (e.g., 1 h) is lost in offline-coupled model systems (Grell et al., 2004; Zhang, 2008). Therefore, an RT-AQF system based on an online-coupled meteorology-chemistry model has a potential to better represent the real atmosphere and thus provides more accurate AQF.

In this study the online-coupled Weather Research and Forecasting model with Chemistry (WRF/Chem, Grell et al., 2005; Fast et al., 2006) version 3.0 with the Model of Aerosol Dynamics, Reaction, Ionization, and Dissolution (MADRID) (Zhang et al., 2004, 2010b,c) (referred to as WRF/Chem-MADRID) is applied for RT-AQF in the southeastern U.S. Compared with the default aerosol model Modal Aerosol Dynamics Model for Europe with the secondary organic aerosol model (MADE/SORGAM) (Ackermann et al., 1998; Schell et al., 2001) used in WRF/Chem for RT-AQF that is based on the modal approach, MADRID uses a sectional representation for particle size distribution and more advanced model treatments. For example, MADE/SORGAM does not simulate thermodynamic equilibrium involving sea-salt and gives very low concentrations of secondary organic aerosol (SOA), whereas MADRID can simulate all major inorganic aerosols and SOA formation with a more advanced module; it therefore gives better agreement with observations (Zhu and Zhang, 2011). Its forecasting skill is evaluated using available observations during May–September, 2009 (i.e., O_3 season). The objectives of this study are to evaluate the forecasting skill of WRF/Chem-MADRID in RT-AQF applications and to identify likely causes of model biases as well as the areas of the improvement.

2. Model description and evaluation protocols

2.1. The RT-AQF systems based on WRF/Chem-MADRID

WRF/Chem-MADRID consists of various options for gas-phase chemistry and aerosol chemistry and microphysics. It treats the major aerosol processes such as the thermodynamic equilibrium for both inorganic and organic species, new particle formation, condensation/evaporation, coagulation, gas/particle mass transfer, dry and wet deposition. It also simulates aerosol direct and semi-direct feedbacks to radiation and planetary boundary layer (PBL) meteorology, as well as its indirect effects on cloud and precipitation formation via aerosol–cloud interaction processes such as aerosol activation by cloud droplets and autoconversion of cloud drops to rain drops. A more detailed description can be found for WRF/Chem in Grell et al. (2005) and Fast et al. (2006), and for WRF/Chem-MADRID in Zhang et al. (2010b). Table S1 in the supplementary material summarizes major physics and chemistry options selected in WRF/Chem-MADRID in this study. The gas-phase chemistry is based on the 2005 Carbon Bond gas-phase mechanism (CB05) (Yarwood et al., 2005). The aqueous-phase chemistry is based on the Carnegie-Mellon University (CMU) bulk aqueous-phase chemical mechanism (Fahey and Pandis, 2001). The aerosol module is based on MADRID 1 (Zhang et al., 2004, 2010b,c). Eight size sections over the PM aerodynamic diameter range of 0.025–11.630 μm are used in MADRID 1. The aerosol activation module is based on Abdul-Razzak and Ghan (2002). Fig. 1 shows a flowchart of the RT-AQF system based on WRF/Chem-MADRID. It was deployed at a horizontal grid resolution of 12 km for an experimental AQF during August 3–10, 2008 (Chuang et al., 2009) and an RT-AQF during May–September, 2009 in this work. The simulated domain (Fig. 2) is divided into nine regions for region-specific statistical evaluation, with region 9 covering essentially ocean and the remaining eight regions covering land areas. The National Center for Environmental Prediction's (NCEP) meteorological forecast is downloaded at 7 PM (Local Standard Time) to initialize a 60-h forecasting cycle. The forecasts during the first 12 h of each 60-h cycle are for spin-up and not used for real-time forecasts. The forecasts during the remaining 48-h are used to provide a two-day forecast. This process of data-downloading and 60-h forecasting is repeated every two days. Daily updates of the AQFs are provided at http://www.meas.ncsu.edu/aqforecasting/

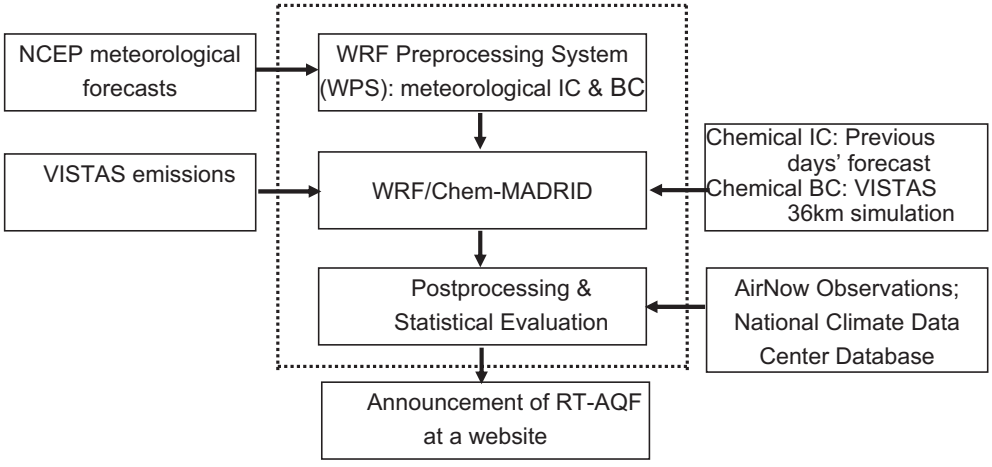

Fig. 1. Flowchart of the RT-AQF system based on WRF/Chem-MADRID (VISTAS denotes the Visibility Improvement State and Tribal Association of the Southeast).

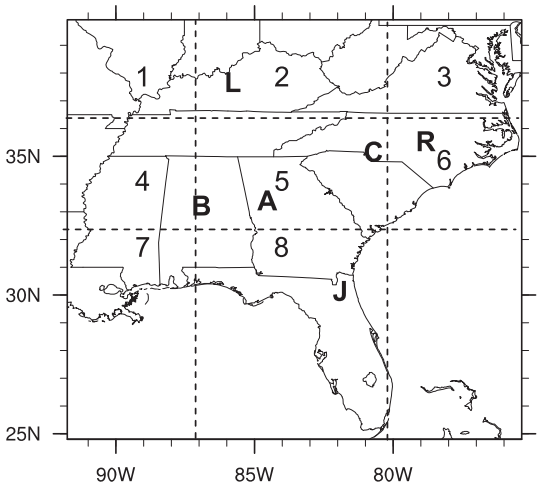

Fig. 2. Simulated domain for RT-AQF. Numbers of 1–9 indicate geographical regions (separated by dash lines) to be evaluated; letters indicate the locations of the selected six urban sites for detailed analyses: A-Atlanta city in Georgia; B-Birmingham city in Alabama; C-Charlotte city in North Carolina; J-Jacksonville city in Florida; L: Louisville city in Kentucky, and R: Raleigh city in North Carolina.

Real_Time.html. The 2009 emissions are projected based on the Visibility Improvement State and Tribal Association of the Southeast's (VISTAS, http://www.vistas-sesarm.org/)'s 2002 emission inventories according to historical growth factors and assumed control strategies (Barnard and Sabo, 2008). The NCEP's meteorological forecasts are used as the initial and boundary conditions for meteorology. VISTAS 2009 36-km CMAQ simulation results and those from the previous day's simulation are used to provide daily chemical boundary and initial conditions (BCONs and ICONs), respectively. For the very first day of the first 60-h forecasting cycle, the model is spin-up for 1-week ahead of the first forecast day using ICONs that represent clean conditions over the U.S. Starting from the second day of this 1-week spin-up, the instantaneous outputs at the last hour on the previous day are used to initialize next day's forecasting simulation. The 4-day averaged BCONs from VISTAS 2009 CMAQ simulations are used for each 60-h forecasting cycle. The first day of the 4-day periods corresponds to the first forecasted day during the 60-h cycle.

2.2. Observational datasets and evaluation protocols

The model performance for major forecasting products such as max 1-h and 8-h average O_3 and 24-h average $PM_{2.5}$ is evaluated against surface observations from the U.S. EPA's AIRNow database (http://www.airnow.gov/). Hourly concentrations of O_3 and $PM_{2.5}$ observed at 380–396 sites and 170–182 sites, respectively, are used. In order to understand the influence of meteorology on AQF, hourly temperature at 2-m (T2), wind speed at 10-m (WS10), and daily total precipitation from the U.S. National Climatic Data Center (NCDC) dataset (http://www.ncdc.noaa.gov/oa/ncdc.html) are also utilized for evaluation.

The model evaluation includes both discrete (Kang et al., 2005; Eder et al., 2006) and categorical measures (Jolliffe and Stephenson, 2003; Kang et al., 2005). In the discrete evaluation, mean bias (MB), normalized mean bias (NMB), root mean square error (RMSE), and normalized mean error (NME) (see their definitions in Table 1) are calculated. In the categorical evaluation, several indices including accuracy (A), critical success index (CSI), probability of detection (POD), bias (B), and false alarm ratio (FAR) are used to evaluate the model's ability to predict exceedances and nonexceedances (Kang et al., 2005):

Table 1
Summary of discrete evaluation for meteorological and chemical variables in May–September of 2009.

		Mean Obs	Mean Sim	MB	RMSE	NMB (%)	NME (%)
hourly T2 (°C)	May	19.8	20.1	0.3	2.7	1.8	7.6
	June	23.9	24.2	0.3	2.5	1.5	5.9
	July	24.1	24.4	0.3	2.4	1.4	5.9
	August	24.4	25.0	0.6	2.4	2.6	6.5
	September	21.5	21.6	0.1	2.3	0.3	6.7
	May–September	22.7	23.1	0.4	2.5	1.5	6.8
hourly WS10 ($m\ s^{-1}$)	May	5.6	4.3	−1.3	3.4	−23.9	35.6
	June	4.7	3.6	−1.1	3.1	−22.6	38.9
	July	4.5	3.5	−1.0	2.9	−21.8	42.1
	August	4.1	3.3	−0.8	2.9	−20.4	41.6
	September	4.5	3.5	−1.0	3.3	−22.5	42.8
	May–September	4.7	3.7	−1.0	3.2	−22.3	40.9
Total daily Precip ($mm\ day^{-1}$)	May	3.5	4.5	1.0	16.1	29.4	175.0
	June	2.4	2.3	−0.1	11.7	−5.7	161.9
	July	2.8	3.8	1.0	15.5	35.7	197.7
	August	2.5	2.9	0.4	14.3	15.5	184.5
	September	3.1	3.3	0.2	16.2	7.9	166.2
	May–September	2.9	3.4	0.5	14.9	18.7	178.0
Max 1-h O_3 (ppb)	May	45.9	49.7	3.8	17.4	8.4	28.3
	June	52.8	53.7	0.9	17.5	1.6	25.2
	July	48.5	54.3	5.8	16.9	12.0	25.9
	August	46.3	54.2	7.9	16.4	17.1	26.7
	September	43.2	47.3	4.0	15.6	9.2	27.5
	May–September	47.3	51.8	4.4	16.8	9.4	26.6
Max 8-h average O_3 (ppb)	May	41.5	43.9	2.4	13.9	5.7	26.1
	June	47.4	47.6	0.2	13.9	0.4	23.2
	July	43.5	47.9	4.4	13.3	10.2	23.6
	August	41.2	48.2	7.0	13.6	17.0	25.7
	September	38.7	42.7	4.0	13.5	10.3	27.3
	May–September	42.5	46.0	3.5	13.6	8.5	25.0
24-h average $PM_{2.5}$ ($\mu g\ m^{-3}$)	May	9.2	8.2	−1.0	4.5	−10.7	36.0
	June	13.5	11.3	−2.2	6.3	−16.2	34.8
	July	12.5	11.4	−1.1	6.0	−8.8	35.9
	August	12.4	12.0	−0.4	6.4	−3.2	36.9
	September	10.2	11.8	1.7	5.9	16.5	42.0
	May–September	11.5	10.0	−0.6	5.9	−5.2	37.0

Note: T2: Temperature at 2 m; WS: Wind Speed; Precip: Precipitation; MB: Mean Bias; RMSE: Root Mean Square Error; NMB: Normalized Mean Bias; NME: Normalized Mean Error.
Mean Bias (MB) $= 1/N \sum_1^N (\text{Sim} - \text{Obs})$,
Root Mean Square Error (RMSE) $= \sqrt{1/N \sum_1^N (\text{Sim} - \text{Obs})^2}$,
Normalized Mean Bias (NMB) $= \sum_1^N (\text{Sim} - \text{Obs}) / \sum_1^N (\text{Obs}) \times 100\%$,
Normalized Mean Error (NME) $= \sum_1^N |\text{Sim} - \text{Obs}| / \sum_1^N (\text{Obs}) \times 100\%$ where Sim, Obs, and N are simulated values, observed values, and the number of observations, respectively.

$$\text{Accuracy } (A) = \left(\frac{b+c}{a+b+c+d}\right) \times 100\% \quad (1)$$

$$\text{Critical Success Index } (\text{CSI}) = \left(\frac{b}{a+b+d}\right) \times 100\% \quad (2)$$

$$\text{Probability Of Detection } (\text{POD}) = \left(\frac{b}{b+d}\right) \times 100\% \quad (3)$$

$$\text{Bias } (B) = \left(\frac{a+b}{b+d}\right) \quad (4)$$

$$\text{False Alarm Ratio } (\text{FAR}) = \left(\frac{a}{a+b}\right) \times 100\% \quad (5)$$

where a, b, c, and d, are the numbers of simulated and observed data pairs at one site at a specific time in the four regions (see Fig. S1 in the supplementary material). They represent forecast

exceedances that did not occur, forecast exceedances that did occur, forecast nonexceedances that did occur, and forecast nonexceedances that did not occur, respectively. *A* indicates the percentage of forecasts that correctly predict both non-exceedances and exceedances. CSI indicates how well both forecast and actual exceedances are predicted. POD indicates the percentage of actual exceedances that are correctly forecasted. *B* indicates that the forecast is overpredicted (>1.0) or underpredicted (<1.0). FAR is the percentage of forecast exceedances that did not occur.

The number of exceedances depends on the choice of threshold values (e.g., Hogrefe et al., 2007; Eder et al., 2009; Djalalova et al., 2010). The latest National Ambient Air Quality Standards (NAAQS) of 120 ppb (revoked for all areas in April 2009 but retain for purposes of the anti backsliding provisions for some areas), 75 ppb (effective on May 27, 2008), and 35 μg m^{-3} (effective in December 2006) provide the threshold values for max 1-h O_3, max 8-h average O_3, and 24-h average $PM_{2.5}$, respectively (http://www.epa.gov/air/criteria.html). For an accurate AQF, it is desirable to have the sum *b* and *c* as close as possible to the total number of forecasts. The frequency of exceedances based on NAAQS is, however, gradually decreasing in most part of the U.S., leading to zero values or not-available (NA) values for CSI, POD, or FAR. The reduced thresholds for categorical evaluation were therefore used in some studies to demonstrate model's capability in forecasting exceedance of those reduced threshold values (e.g., Hogrefe et al., 2007), although higher thresholds were used in some earlier air quality forecasts several years ago (e.g., Kang et al., 2005; Lee et al., 2008; Eder et al., 2009). For example, Hogrefe et al. (2007) used two sets of thresholds, 85 and 65 ppb for max 8-h average O_3 and 45.5 and 15.5 μg m^{-3} for 24-h average $PM_{2.5}$, which are equivalent to air quality indices of 100 and 50, respectively. In addition, lower threshold values of 60 ppb and 80 ppb were used for forecasted max 1-h O_3 in regions with lower O_3 mixing ratios such as Australia and the Iberian Peninsula (e.g., Cope et al., 2004; Cope and Hess, 2005; Jiménez et al., 2006). In this work, the thresholds of 80 ppb, 60 ppb, and 15 μg m^{-3} are used for max 1-h O_3, max 8-h average O_3, and 24-h average $PM_{2.5}$, respectively, based on the same or similar lower threshold values used in literature (e.g., Hogrefe et al., 2007; Djalalova et al., 2010). These choices reflect the effectiveness of the emission reductions since earlier applications of other AQF models.

3. Evaluation of WRF/Chem-MADRID

3.1. Discrete evaluation

Fig. 3 shows the overlay plots of 5-month mean daily max 8-h average O_3 and 24-h average $PM_{2.5}$ with AIRNow observations. O_3 overpredictions are most apparent in most areas of Kentucky and Tennessee, southern areas of Indiana, Illinois, and Ohio, and the Appalachian Mountains region. Table 1 summarizes discrete evaluation. The monthly NMBs are 1.6–17.1% for max 1-h O_3 and 0.4–17% for max 8-h average O_3, with the best performance in June and the worst in August. The O_3 overpredictions are likely due to underpredicted WS10 with MBs of −1.3 to −0.8 m s^{-1}, overpredicted T2 with MBs of 0.1–0.6 °C, inaccuracies in other meteorological variables such as PBL height, and uncertainties in precursor emissions. The 5-month average $PM_{2.5}$ concentrations agree well with the observations in the northwest and central portions of the domain and around the Appalachian Mountains but they are underpredicted in some south and east regions of the domain. In addition to uncertainties in emissions, such underpredictions may be caused by overpredictions in T2 and Precipitation. The monthly NMBs are −16.2 to 16.5% for 24-h $PM_{2.5}$ concentrations, with the best performance in August and the worst in September.

The monthly-mean MBs of T2, WS10, Precip, max 8-h average O_3, and 24-h average $PM_{2.5}$ in regions 1–8 (see Fig. 2) are shown in Fig. 4. The monthly-mean O_3 mixing ratios are overpredicted in the entire domain during the 5-month period with the exception of region 1 in May and regions 1, 2, and 4 in June and region 3 in September where underpredictions occur. Domain-wide underpredictions also occur primarily near the north boundary during 26 days out of the 5-month period (i.e., May 17–23, May 30–June 2, June 21–July 1, and September 2–5). In addition to uncertainties in precursor emissions, the O_3 overprediction in most regions in most months is likely caused by positive biases in T2 in most regions and the negative biases in WS10 in most regions. The O_3 underpredictions in regions 1, 2, and 4 in May and June could be due partly to the uncertainties in lateral boundary conditions (LBCs). The observed prevailing wind during the two months was accompanied with anticyclones moving from the north and northwest boundaries of the domain (http://www.hpc.ncep.noaa.gov/dailywxmap/index.html). The impact of such an incoming

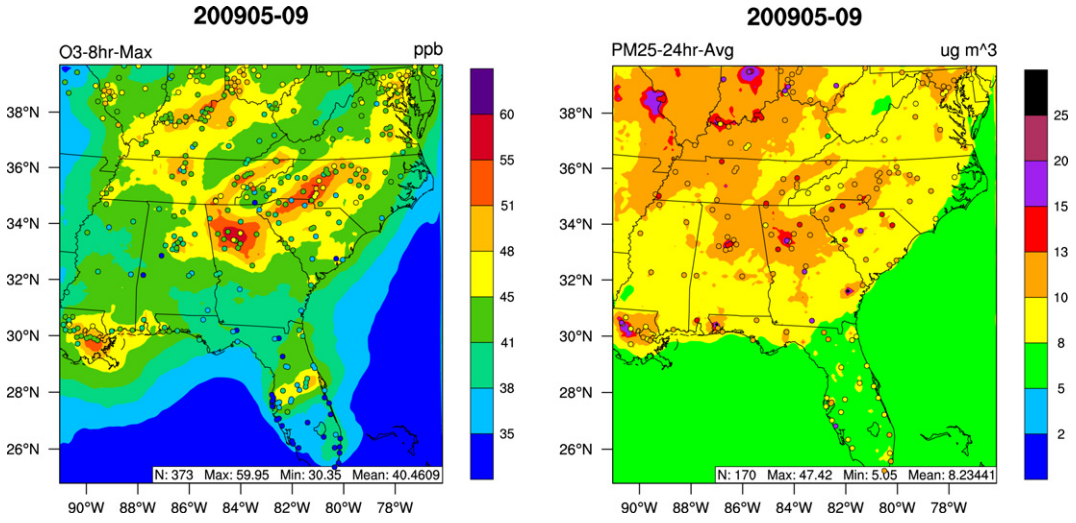

Fig. 3. Five-month (May–September 2009) mean spatial distribution of concentrations of max 8-h average O_3 (left), and 24-h average $PM_{2.5}$ (right) (circles indicate observations from AIRNow, http://www.epa.gov/airnow).

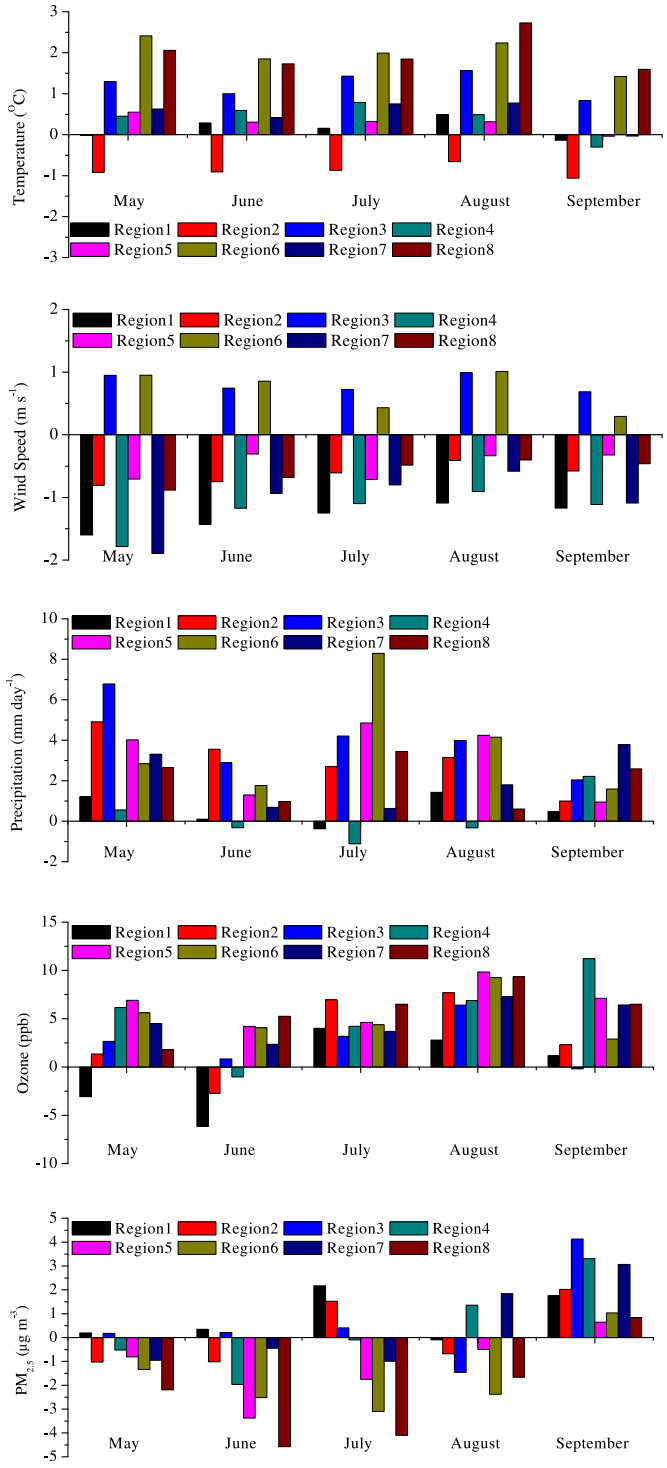

Fig. 4. Monthly-mean MBs of temperature at 2-m, wind speed at 10-m, daily total precipitation, and concentrations of max 8-h average O_3 and 24-h average $PM_{2.5}$ in different regions (see definition of regions 1–8 in Fig. 2) for May–September 2009.

flow on O_3 forecast is not well captured over the 12-km domain. As indicated by Otte et al. (2005), uncertainties exist for LBCs because of the lack of real-time chemical observations. This problem could be improved by using either a larger simulation domain or two nested domains for RT-AQF but at the expense of increased computational costs (Lee et al., 2008; Eder et al., 2009).

As shown in Fig. 4, monthly-mean $PM_{2.5}$ concentrations are slightly overpredicted in regions 1 and 3 in May and June, regions 1, 2 and 3 in July, regions 4 and 7 in August, and all regions in September, and underpredictions occur in other regions during other months. While these over- or under-predictions may be partly caused by inaccurate emissions of PM precursors and primary PM, biases in meteorological predictions can propagate into PM predictions. High simulated $PM_{2.5}$ concentrations usually occurred in regions 1, 2, and 4 at times when anticyclones and cold fronts moved from the north or west (e.g., May 8–9, 14, 16–17, July 13–14, 17–18, 21–23, 26–27, August 13, September 22–24) or a stationary front appeared near the north boundary (e.g., June 13–14). For regions 3 and 7, overpredicted $PM_{2.5}$ concentrations occurred in Washington D.C. and New Orleans areas when WS10 was underpredicted. The daily bias of simulated $PM_{2.5}$ concentrations in regions 2–4 and 7 is larger than 2 $\mu g\ m^{-3}$ during most days in September The simulated monthly-mean PBL heights in September are lower by 112–146 m (by 10–40%) than those in other months, possibly due to unique urban structures unrepresented in WRF (Chen et al., 2007). The effect of a shallow PBL on $PM_{2.5}$ dominates over that of overpredicted Precipitation, causing overpredicted $PM_{2.5}$ concentrations in September. $PM_{2.5}$ concentrations are underpredicted in most regions in May–August (Fig. 4), due likely to overpredictions in T2 and Precipitation and uncertainties in emissions. Regions 5, 6, and 8 have higher negative MBs than other regions. When anticyclones and fronts move from the north, the model tends to significantly overpredict precipitation near the Appalachian Mountains. This, coupled with overpredictions in T2, leads to underpredicted $PM_{2.5}$ in regions 5 and 6. Overpredicted precipitation around the southern Georgia and Florida also causes the underprediction of $PM_{2.5}$ in region 8.

Fig. 5 shows simulated and observed daily max 8-h average O_3 mixing ratios at the six urban sites. The model captures a significant fraction of 8-h O_3 episodes higher than 50 ppb but overpredicts those below 50 ppb, leading to positive biases at urban sites. The O_3 overpredictions at Birmingham and Atlanta may be caused by inaccurate precursor emissions, overpredicted T2, and underpredicted WS10. The U.S. EPA is considering to tighten the existing NAAQS for max 8-h average O_3 from 75 ppb to 60–70 ppb (U.S. EPA, 2010). The observations at these sites during the 5-month period are >60 ppb on some days at all sites, indicating a potential increase in the non-attainment areas if the proposed new standard is adopted in 2011.

Fig. 6 shows simulated and observed 24-h average $PM_{2.5}$ concentrations at urban sites. $PM_{2.5}$ predictions generally agree well with observations except at Birmingham in region 5 where overpredictions occur during most of time. The underpredictions in WS10 may lead to higher $PM_{2.5}$ concentrations, although such an effect may be partially compensated by overpredictions in precipitation near Birmingham in region 5 (Fig. 4). In addition to meteorological factors, overestimated emissions may explain $PM_{2.5}$ overpredicions at this site. Gupta and Christopher (2008) reported that the observed $PM_{2.5}$ concentrations at Birmingham have been declining since 2000, which may not be well represented in the VISTAS emission inventory. Unlike other cities, $PM_{2.5}$ levels in Louisville in region 2 are sometimes underpredicted, which may be caused by lower LBCs used and the dominant effect of overpredicted precipitation. As shown in Table S2, the model performs better for O_3 in rural/suburban areas than urban/coastal areas and for $PM_{2.5}$ in urban/suburban areas than rural/coastal areas, due to larger impacts of inaccurate emissions of O_3 precursors in urban areas, larger underestimates in NH_3 emissions in rural areas, and the model limitations in capturing sea breezes in coastal areas at a horizontal grid resolution of 12-km.

Compared with performance of current RT-AQF models (e.g., McHenry et al., 2004; Kang et al., 2005; McKeen et al., 2005, 2007; Hogrefe et al., 2007; Chen et al., 2008; Yu et al., 2008; Eder et al.,

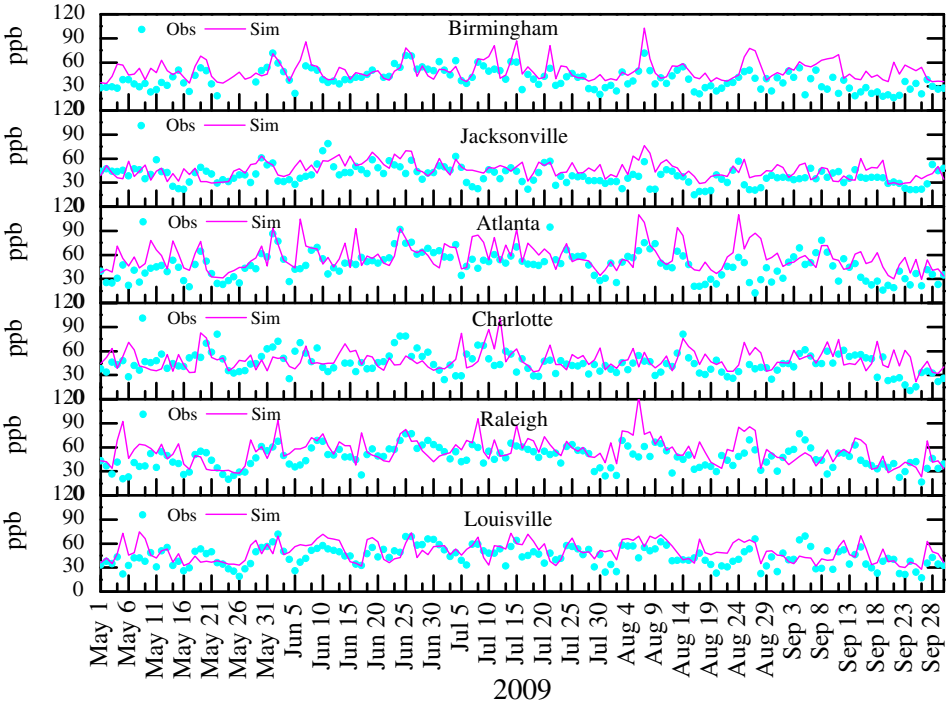

Fig. 5. Simulated and observed daily max 8-h average O_3 mixing ratios at representative urban sites during May–September 2009 (see site locations in Fig. 2). The observational data were obtained from AIRNow, http://www.epa.gov/airnow. Louisville is in Region 2, Atlanta, Birmingham, and Charlotte are in Region 5, Raleigh is in Region 6, Jacksonville is in Region 8.

2009), that of WRF/Chem-MADRID for max 1-h/8-h O_3 and 24-h/hourly average $PM_{2.5}$ is either comparable or better. For example, Yu et al. (2007, 2008) reported NMBs of 11.9–22.6% and −21% for forecasted max 8-h average O_3 and 24-h average $PM_{2.5}$, respectively, using Eta/CMAQ during July–August 2004 and Eder et al. (2009) reported NMBs of 16.5–25.2% for forecasted max 8-h average O_3 using WRF/CMAQ over the eastern U.S. Chen et al. (2008) reported NMBs of 6% and 17–32% for forecasted max 8-h

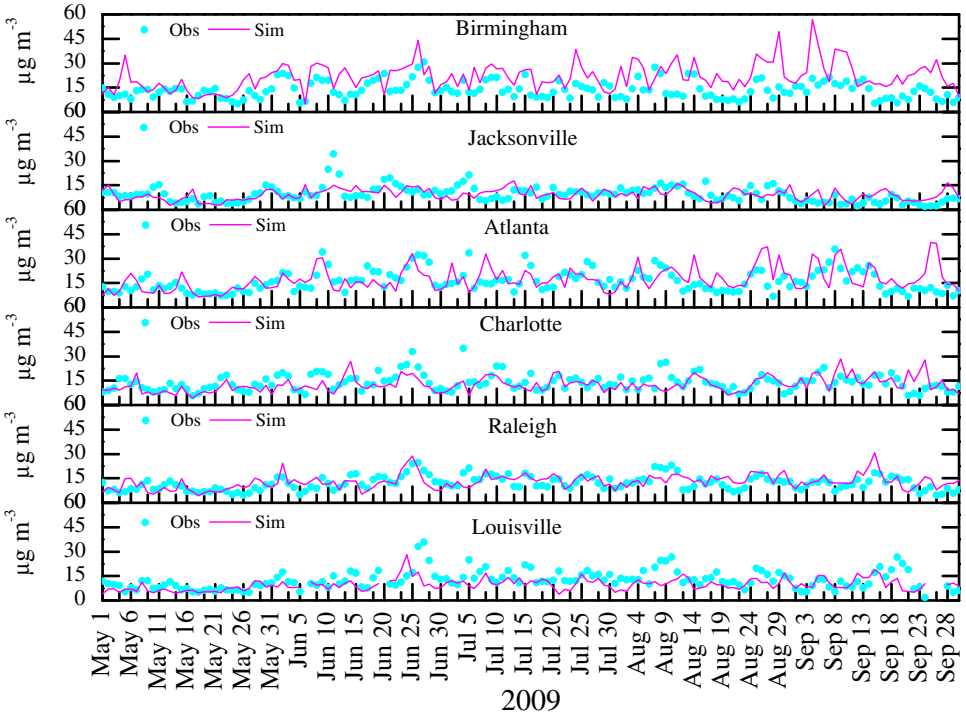

Fig. 6. Simulated and observed 24-h average $PM_{2.5}$ concentrations at representative urban sites for May–September 2009 (see site locations in Fig. 2). The observational data were obtained from AIRNow, http://www.epa.gov/airnow. Louisville is in Region 2, Atlanta, Birmingham, and Charlotte are in Region 5, Raleigh is in Region 6, Jacksonville is in Region 8.

average O_3 and 24-h average $PM_{2.5}$, respectively, using the Air Indicator Report for Public Access and Community Tracking (AIRPACT) that is based on MM5/CMAQ during August–September 2004 over the Pacific Northwest.

3.2. Categorical evaluation

Table 2 summarizes categorical evaluation results. For max 1-h and 8-h average O_3, the monthly-mean *A* values are high, 92.2–97.9% and 80.0–91.8%, respectively, with the highest in September, indicating an overall good accuracy for forecast non-exceedances. The values of CSI and POD are low, ranging from 0.4 to 7.7% and 5.6–43.0% for max 1-h average O_3, and 2.5–17.5%, and 7.2–56.8% for max 8-h average O_3, respectively. The values of a are much higher than the values of *b* for max 1-h and 8-h average O_3 in all months, indicating a dominance of overpredictions. CSI and POD in September are the lowest among all months. POD in August is the highest. The monthly-mean *B* values are 2.6–11.9 and 1.0–2.8, and monthly-mean FAR values are 90.0–99.5% and 73.5–96.2%, for max 1-h and 8-h average O_3, respectively. *B* values are the highest in September for max 1-h average O_3 and in August for max 8-h average O_3. The *b* value is the lowest in September, leading to the highest FAR values for both max 1-h and 8-h average O_3. Similarly, the FAR values are the lowest in June due to the highest *b* values. For 24-h average $PM_{2.5}$, monthly-mean *A*, CSI, POD, *B*, and FAR are 70.8–91.9%, 10.8–26.7%, 16.0–47.8%, 0.5–1.3, and 38.6–74.7%, respectively. Unlike O_3, *A* and FAR are the highest and CSI and POD are the lowest in May for $PM_{2.5}$. *A* is the lowest in both June and August. FAR is the lowest in June. *B* is the highest in September with a value of 1.3, indicating that $PM_{2.5}$ is overpredicted in this month. *B* values are less than 1 for other months, indicating underpredicted $PM_{2.5}$ concentrations. As indicated in Table S2, the model gives higher CSI, POD, and *B* for max 1-h O_3 in urban areas but a more uniform categorical performance for max 8-h O_3 in all areas. The model gives higher CSI, POD, and *B* and lower FAR and *A* for 24-h average $PM_{2.5}$ in urban/suburban areas. *A* and FAR are the highest and CSI, POD and *B* the lowest in coastal areas.

4. Sensitivity studies

4.1. The impact of biogenic emissions

In addition to the uncertainty in the projected agricultural NH_3 emissions and anthropogenic emissions of specific industrial sources, other uncertainties arise from biogenic VOC (BVOC) emissions that are influenced by real-time meteorological factors such as temperature, humidity, and solar radiation. WRF/Chem offers two options to simulate biogenic emissions: offline and online. The offline BVOC emissions from the VISTAS emission inventories are used in RT-AQF results described previously. To study the sensitivity of model performance to BVOC emissions, a sensitivity simulation is conducted for July, 2009 by replacing offline BVOC emissions with an online BVOC emission scheme that is based on Guenther et al. (1993) and Simpson et al. (1995) (referred to as the Guenther scheme). In the Guenther scheme, emissions of isoprene, monoterpenes, other VOCs (OVOCs) including alkanes, xylene, alkenes, ketones, aldehyde, formaldehyde, ethane, organic acid from plants, and nitrogen oxide (NO) from soil are included. Their emission rates are calculated according to the types of plants, temperature, solar radiation, and occurrence of rain. In the default Guenther scheme in WRF/Chem, the monoterpenes emission is allocated to isoprene and OVOCs (Grell et al., 2005; Fast et al., 2006) because the Guenther scheme is only coupled with the gas-phase mechanism of the Regional Acid Deposition Model (RADM) that does not include monoterpenes. Since CB05 used in WRF/Chem-MADRID explicitly simulates monoterpenes, the Guenther scheme is modified to allocate monoterpenes emissions to monoterpenes (rather than isoprene and OVOCs) in this study (referred to as the modified Guenther scheme). The modified Guenther scheme results in lower isoprene and higher monoterpenes emissions than the VISTAS 2009 offline biogenic emissions and thus lower (by up to 6 ppb) and higher (by up to 3 ppb) mixing ratios of isoprene and monoterpenes, respectively, in the southeastern U.S., as shown in Fig. S2. Several studies (Kang et al., 2004; Zhang et al., 2009) have shown that most areas in the Southeastern U.S. are NO_x-limited in summer. Lower online isoprene emissions make more HO_x radicals available for the conversion of NO to NO_2, which increases O_3 formation in a large areas in the domain (e.g., regions 4–6), with a domain-wide mean increase of 0.38 ppb (or by 8.9%) (see Fig. S3). Simulated O_3 mixing ratios with online BVOCs emissions, however, decrease in several regions (e.g., regions 1–2 and the southern portion of region 8). Many studies have shown that monoterpenes and isoprene are major precursors of SOA formation (e.g., Kroll et al., 2006; Zhang et al., 2007). The increased monoterpenes mixing ratios from the sensitivity simulation lead to an increase in SOA that dominates over the decrease in SOA due to lower isoprene mixing ratios, resulting in higher domain-wide simulated $PM_{2.5}$ concentrations by $\sim$0.6 μg m^{-3} (or by 6.2%).

Table 2
Summary of categorical evaluation for O_3 and $PM_{2.5}$ in May–September of 2009.

	Threshold	Period	*A* (%)	CSI (%)	POD (%)	*B*	FAR (%)	*a*	*b*	*c*	*d*
Max 1-h O_3 (ppb)	80 ppb	May	94.6	2.0	22.0	10.0	97.7	576	13	10,914	46
		June	92.3	7.7	25.5	2.5	90.0	658	73	10,332	213
		Jul	92.9	6.0	40.8	6.2	93.4	754	53	10,766	77
		August	92.2	4.8	43.0	8.3	94.8	844	46	10,707	61
		September	97.9	0.4	5.6	11.9	99.5	218	5	11,024	22
		May–September	94.0	5.2	31.3	5.3	94.1	3050	190	53,743	419
Max 8-h average O_3 (ppb)	60 ppb	May	88.3	12.5	29.1	1.6	82.0	863	189	9813	460
		June	80.0	15.1	26.0	1.0	73.5	1100	395	8470	1123
		Jul	83.9	14.8	41.7	2.2	81.4	1389	318	9278	444
		August	84.5	17.5	56.8	2.8	79.7	1474	374	9179	285
		September	91.8	2.5	7.2	1.9	96.2	594	27	9901	300
		May–September	85.6	14.0	33.3	1.7	80.6	5420	1303	46,641	2612
24-hraverage $PM_{2.5}$ (μg m^{-3})	15 μg m^{-3}	May	91.9	10.8	16.0	0.6	74.7	160	54	4655	284
		June	69.9	26.7	32.1	0.5	38.6	341	541	2904	1143
		Jul	70.8	19.2	27.1	0.7	60.1	539	358	3282	965
		August	69.9	21.1	30.0	0.7	58.2	571	409	3137	955
		September	78.8	25.8	47.8	1.3	64.1	643	362	3482	395
		May–September	76.2	22.3	31.5	0.7	56.6	2254	1724	17,460	3742

1. *A*: Accuracy; CSI: Critical success index; POD: probability of detection; *B*: bias: FAR: False alarm ratio.
2. *a*, *b*, *c*, *d*, are the number of simulated and observed data pairs at one site for a specific time in the four regions shown in Fig. S1.

Table 3
Comparison of discrete evaluation of the baseline RT-AQF with offline biogenic emissions and the sensitivity simulations with online biogenic emissions based on the modified Guenther scheme, and modified boundary conditions in July 2009.

		Mean Obs	Mean Sim	MB	RMSE	NMB (%)	NME (%)
Max 1-h O_3 (ppb)	Offline BVOCs	48.5	54.4	5.9	16.9	12.1	25.9
	Online BVOCs		54.4	5.9	16.9	12.1	26.0
	Modified LBCs		50.3	1.8	15.6	3.7	24.3
Max 8-h average O_3 (ppb)	Offline BVOCs	43.5	47.9	4.4	13.3	10.2	23.6
	Online BVOCs		48.1	4.6	13.4	10.5	23.9
	Modified LBCs		44.4	0.9	12.6	2.0	22.3
24-h average $PM_{2.5}$ ($\mu g\ m^{-3}$)	Offline BVOCs	12.5	11.4	−1.1	6.0	−8.9	35.9
	Online BVOCs		12.3	−0.3	6.0	−1.7	35.4
	Modified LBCs		12.8	0.3	6.1	2.8	36.5

Obs: Observation; Sim: Simulation; MB: Mean Bias; RMSE: Root Mean Square Error; NMB: Normalized Mean Bias; NME: Normalized Mean Error; BVOCs: Biogenic Volatile Organic Carbons; LBCs: Lateral Boundary Conditions.

Table 3 compares model performance using offline and online BVOC emissions in July 2009. The use of online BVOC emissions slightly reduces the domain-wide mean MB and NMB for $PM_{2.5}$ but slightly increases those for max 8-h O_3. As shown in Fig. 7, the online BVOC emission reduces the positive bias of O_3 in regions 1 and 2, but leads to higher MBs for O_3 in regions 5–8, where isoprene emissions are reduced. The use of online BVOC emissions reduces the negative MBs and NMBs for $PM_{2.5}$ in regions 5–8, where monoterpenes emissions are enhanced. $PM_{2.5}$ predictions in regions 1–4 are worse, due primarily to increased SOA resulted from increased monoterpenes. In addition, in July when fronts did not influence the domain, wind direction was usually from southeast and south. Enhanced levels of PM and/or its precursors with online BVOC emissions may be transported from regions 5–8 into regions 1–4, contributing to overpredictions for these four regions.

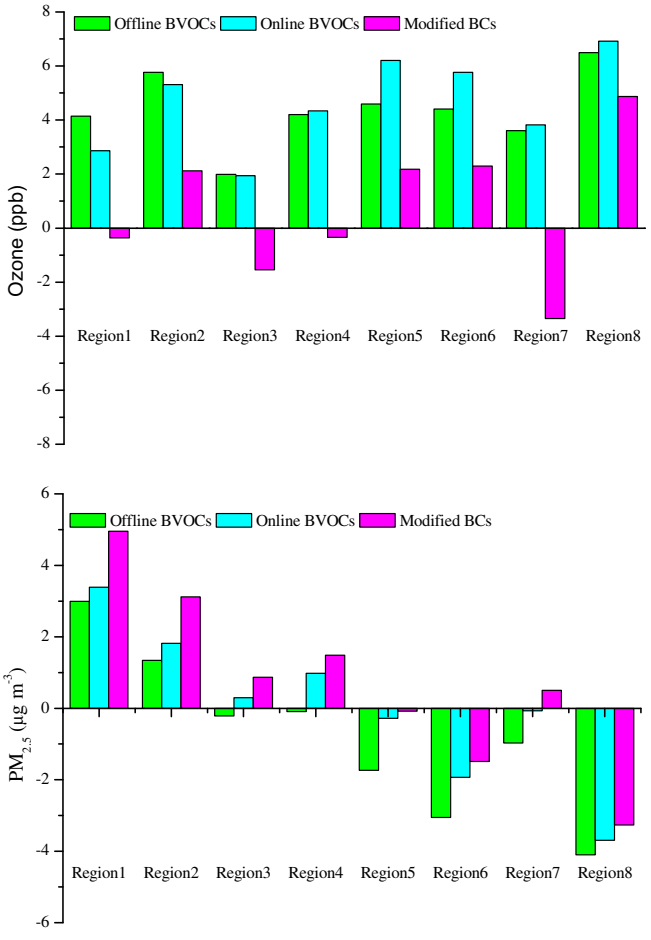

Fig. 7. July 2009 monthly-mean bias of concentrations of daily max 8-h average O_3 (upper) and 24-h average $PM_{2.5}$ (lower) from simulations with offline (baseline) and online (Guenther scheme) biogenic volatile compound emissions, and modified boundary condition (labeled as offline BVOCs, online BVOCs, and modified BCs, respectively).

4.2. The impact of lateral boundary conditions

In this sensitivity simulation, the concentrations of O_3 and $PM_{2.5}$ at all four lateral boundaries used in July 2009 baseline RT-AQF simulation are decreased by 20% and increased by 20%, respectively. As shown in Fig. S4, the overprediction of O_3 is reduced in most areas with a domain-wide mean reduction of 2.1 ppb (or by −4.8%) except the south of Georgia and north of Florida and southeast of South Carolina. The largest reductions occurred in Louisiana and Mississippi. In July, there were still intermittent fronts moving from north to south or being stagnant in the domain. In areas ahead of the fronts, prevailing winds in Mississippi and Louisiana tended to be from the west and southwest along the Gulf coastal area. With reduced LBCs for O_3, less incoming O_3 titrate less NO at night to form less NO_2 locally that leads to less local O_3 formation during daytime. This effect is more obvious near the west boundary and especially in New Orleans. On the other hand, excessive NO as a result of less O_3 titration in Mississippi and Louisiana can be transported to the downwind area with the front and enhance O_3 formation in south of Georgia, north of Florida and southeast of South Carolina. Another possible reason leading to O_3 increase in those areas is the decrease of the photolysis rate of O_3 as a result of increased $PM_{2.5}$ LBCs due to the feedbacks of aerosols into photolysis. As shown in Fig. 7, the predictions of O_3 in all regions are improved (note that O_3 mixing ratios in region 7 change from overprediction to underpredictions, particularly in New Orleans, but with lower absolute MB). For $PM_{2.5}$, with increased LBCs, MBs in regions 1–4 are increased but they are reduced in regions 5–8, leading to a net decrease in bias for domain-wide $PM_{2.5}$ predictions. Domain-wide $PM_{2.5}$ concentration increase by up to 1.3 $\mu g\ m^{-3}$ (or by 16.6%). As shown in Table 3, the model performance with modified LBCs is improved for O_3 and $PM_{2.5}$ predictions.

5. Conclusions

In this study, an RT-AQF system has been developed based on WRF/Chem-MADRID and deployed for RT-AQF in the southeastern U.S. during May–September, 2009. Forecasted max 1-h and 8-h average O_3 mixing ratios are overpredicted while forecasted 24-h average $PM_{2.5}$ concentrations are underpredicted. The overprediction of O_3 is possibly caused by uncertainties in emissions (in particular, BVOC emissions), inaccuracies in the predicted meteorological variables (e.g., T2, WS10) and uncertainties in LBCs. The underprediction of $PM_{2.5}$ is likely due to the uncertainties in the emissions of precursors such as NH_3 and BVOC emissions, overpredictions of precipitation, and imperfect LBCs. The online BVOC emissions calculated based on the modified Guenther scheme can help improve domain average $PM_{2.5}$ and O_3 and $PM_{2.5}$ forecast in some regions, but may give larger biases for other regions. Adjusted LBCs reduce domain-wide overpredictions of O_3 but cause the underpredictions of O_3 at urban cities near the boundaries. They reduce domain-wide underpredictions of $PM_{2.5}$ but cause larger biases for some regions.

While the RT-AQF model based on WRF/Chem-MADRID demonstrates a promising forecasting skill that is consistent with

current RT-AQF models, several aspects can be improved. For example, online BVOC emissions that reflect the impact of real-time meteorological conditions should be used for future RT-AQF, the emission factors of isoprene and other BVOCs in the Guenther scheme can be improved based on latest measurements. The impact of real-time meteorology on other meteorologically-dependent emissions such as NH_3 emissions and parameters such as plume rise should also be considered. The SOA module can be further improved to include SOA formation via the condense-phase oligomerization and aqueous-phase oxidation of glyoxal and methylglyoxal in cloud droplets, which has been shown to play an important role (Carlton et al., 2008). For the RT-AQF application, when additional resources available, the current 12-km domain may be expanded to reduce the impact of imperfect LBCs or resolved with finer grid for RT-AQF in sub-domain within the 12-km domain (Tie et al., 2010). The current chemical LBCs based on the 2009 VISTA CMAQ simulation can be replaced by those derived from the real-time chemical composition forecasts of a global AQF model (e.g., the one developed in the Monitoring Atmospheric Composition & Climate (MACC) project, http://www.gmes-atmosphere.eu) or a regional AQF model (e.g., the NOAA Earth System Research Laboratory WRF/Chem) that covers a larger domain than the current 12-km domain. The underprediction of wind speed and overprediction of precipitation may be improved by using improved dynamics, cloud microphysics, and radiation schemes and/or testing alternative options and combinations to obtain an optimal configuration for model representations of meteorological conditions in the southeastern U.S. Finally, some studies have attempted to improve the forecasting results using several approaches. For example, Guillas et al. (2008) used the Model Diagnostic Correction (MDC) approach and reduced the errors of forecast by up to 25%. Kang et al. (2008) applied bias adjustment techniques of the hybrid forecast and the Kalman filter method to improve the systematic positive bias in the O_3 predictions. These bias correction approaches may be explored to further improve the model's forecasting skill.

Acknowledgments

This work was performed under the NSF Career Award No. ATM-0348819, Memorandum of Understanding between the U.S. Environmental Protection Agency (EPA) and the U.S. Department of Commerce's National Oceanic and Atmospheric Administration (NOAA) and under agreement number DW13921548, and the EPA-Science to Achieve Results (STAR) program (#R83337601). We acknowledge observational datasets from the U.S. EPA AIRNow and Department of Commerce's National Climatic Data Center (NCDC). We also thank Nan Zhang, a graduate student at NCSU, for her help in some data processing and plotting.

Appendix. Supplementary material

Supplementary data associated with this article can be found, in the online version, at doi:10.1016/j.atmosenv.2011.06.071.

References

Abdul-Razzak, H., Ghan, S.J., 2002. A parameterization of aerosol activation. 3. Sectional representation. Journal of Geophysical Research-Atmosphere 107 (D3). doi:10.1029/2001JD000483.

Ackermann, I.J., Hass, H., Memmesheimer, M., Ebel, A., Binkowski, F.S., Shankar, U., 1998. Modal aerosol dynamics model for Europe: development and first applications. Atmospheric Environment 32, 2981–2999.

Barnard W.R., Sabo E., 2008. Documentation of the Base G2 and Best & Final 2002 Base Year, 2009 and 2018 Emission Inventories for VISTAS, Final Report prepared by MACTEC Engineering and Consulting, Inc. for the Visibility Improvement State and Tribal Association of the Southeast (VISTAS), March 14.

Cai, C., Hogrefe, C., Katsafados, P., Kallos, G., Beauharnois, M., Schwab, J.J., Brune, W.H., Zhou, X., He, Y., Demerjian, K.L., 2008. Performance evaluation of air quality forecast modeling system for a summer and winter season – photochemical oxidants and their precursors. Atmospheric Environment 42, 8585–8599.

Carlton, A.G., Turpin, B.J., Altieri, K.E., Seitzinger, S.P., Mathur, R., Roselle, S.J., Weber, R.J., 2008. CMAQ model performance enhanced when in-cloud SOA is included: comparisons of OC predictions with measurements. Environmental Science & Technology 42 (23), 8798–8802.

Chen, J., Vaughan, J., Avise, J., O'Neill, S., Lamb, B., 2008. Enhancement and evaluation of the AIRPACT ozone and $PM_{2.5}$ forecast system for the Pacific Northwest. Journal of Geophysical Research-Atmosphere 113 (D14305). doi:10.1029/2007JD009554.

Chen, J., Zheng, Y.-G., Deng, L.-T., 2007. Effects of urban buildings on 3-dimensional PBL structures: WRF simulation study. Journal of Peking University (Beijing Da Xue Xue Bao (Ziran Kexue)/Acta Scientiarum Naturalium Universitatis Pekinensis) 43 (3), 343–350.

Chuang, M.-T., Pan Y., Zhang Y., Kang D., 2009. Initial Application of WRF/Chem-MADRID for Real-Time Air Quality Forecasting over the Southeastern United States, poster presentation at the 8th annual CMAS meeting, October 19–21, 2009, Chapel Hill, NC.

Cobourn, W.G., 2007. Accuracy and reliability of an automated air quality forecast system for ozone in seven Kentucky metropolitan area. Atmospheric Environment 41, 5863–5875.

Cope, M.E., Hess, G.D., Lee, S., Tory, K., Azzi, M., Carras, J., Lilley, W., Manins, P.C., Nelson, P., Ng, L., Puri, K., Wong, N., Walsh, S., Young, M., 2004. The Australian air quality forecasting system. Part I: project description and early outcomes. Journal of Applied Meteorology 43, 649–662.

Cope, M.E., Hess, G.D., 2005. Air quality forecasting: a review and comparison of the approaches used internationally and in Australia. Clean Air and Environmental Quality 39 (1), 39–45.

Djalalova, I., Wilczak, J., McKeen, S., Grell, G., Peckham, S., Pagowski, M., Delle-Monache, L., McQueen, J., Tang, Y., Lee, P., McHenry, J., Gong, W., Bouchet, V., Mathur, R., 2010. Ensemble and bias-correction techniques for air quality model forecasts of surface O_3 and $PM_{2.5}$ during the TEXAQS-II experiment of 2006. Atmospheric Environment, 44, 455–467, doi:10.1016/j.atmosenv.2009.11.007.

Eder, B., Kang, D., Mathur, R., Yu, S., Schere, K., 2006. An operational evaluation of the Eta-CMAQ air quality forecasting model. Atmospheric Environment 40, 4894–4905.

Eder, B., Kang, D., Mathur, R., Pleim, J.E., Yu, S., Otte, T., Pouliot, G., 2009. A performance evaluation of the national air quality forecast capability for the summer of 2007. Atmospheric Environment 43, 2312–2320.

Fahey, K.M., Pandis, S.N., 2001. Optimizing model performance: variable size resolution in cloud chemistry modeling. Atmospheric Environment 35, 4471–4478.

Fast, J.D., Gustafson Jr., W.I., Easter, R.C., Zaveri, R.A., Barnard, J.C., Chapman, E.G., Grell, G.A., 2006. Evolution of ozone, particulates, and aerosol direct forcing in an urban area using a new fully-coupled meteorology, chemistry, and aerosol model. Journal of Geophysical Research-Atmosphere 111 (D21305). doi:10.1029/2005JD006721.

Flemming, J., Inness, A., Flentje, H., Huijnen, V., Moinat, P., Schultz, M.G., Stein, O., 2009. Coupling global chemistry transport models to ECMWF's integrated forecast system. Geoscience Model Development Discussions 2, 763–795.

Grell, G.A., Knoche, R., Peckham, S.E., McKeen, S.A., 2004. Online versus offline air quality modeling on cloud-resolving scales. Geophysical Research Letters 31 (L16117). doi:10.1029/2004GL020175.

Grell, G.A., Peckham, S.E., Schmitz, R., McKeen, S.A., Frost, G., Skamarock, W.C., Eder, B., 2005. Fully coupled "online" chemistry within the WRF model. Atmospheric Environment 39, 6957–6975.

Gualtieri, G., 2010. Implementing an operational ozone forecasting system based on WRF/CALMET/CALGRID models: a 5-month case study over Tuscany, Italy. Water, Air, and Soil Pollution 209 (1–4), 269–293.

Guenther, A.B., Zimmerman, P.R., Harley, P.C., Monson, R.K., Fall, R., 1993. Isoprene and monoterpene emission rate variability: model evaluations and sensitivity analyses. Journal of Geophysical Research-Atmosphere 98D, 12609–12617.

Guillas, S., Bao, J., Choi, Y., Wang, Y., 2008. Statistical correction and downscaling of chemical transport model ozone forecasts over Atlanta. Atmospheric Environment 42, 1338–1348.

Gupta, P., Christopher, S.A., 2008. Seven year particulate matter air quality assessment from surface and satellite measurement. Atmospheric Chemistry and Physics 8, 3311–3324.

Hogrefe, C., Hao, W., Civerolo, K., Ku, J.Y., Sistla, G., Gaza, R.S., Sedefian, L., 2007. Daily simulation of ozone and fine particulates over New York State: findings and challenges. Journal Applied Meteorology 46, 961–979.

Jiménez, P., Jorba, O., Parra, R., Baldasano, J.M., 2006. Evaluation of MM5-EMICAT2000-CMAQ performance and sensitivity in complex terrain: high-resolution application to the northeastern Iberian Peninsula. Atmospheric Environment 41, 5056–5072. doi:10.1016/j.atmosenv.2005.12.060.

Jolliffe, I.R., Stephenson, D.B., 2003. Forecast Verification: A Practitioner's Guide in Atmospheric Science. John Wiley & Sons, Ltd., West Sussex, English. 240 pp.

Kang, D., Aneja, V.P., Mathur, R., Ray, J.D., 2004. Observed modeled VOC chemistry under high VOC/NO_x conditions in the Southeast United States national parks. Atmospheric Environment 38, 4969–4974.

Kang, D., Eder, B.K., Stein, A.F., Grell, G.A., Peckham, S.E., McHenry, J., 2005. The New England air quality forecasting pilot program: development of an evaluation protocol and performance benchmark. Journal of the Air & Waste Management Association 55, 1782–1796.

Kang, D., Mathur, R., Rao, S.T., Yu, S., 2008. Bias adjustment techniques for improving ozone air quality forecasts. Journal of Geophysical Research-Atmosphere 113 (D23308). doi:10.1029/2008JD010151.

Kroll, J.H., Ng, N.L., Murphy, S.M., Flagan, R.C., Seinfeld, J.H., 2006. Secondary organic aerosol formation from isoprene photooxidation. Environmental Sciences & Technology 40, 1869–1877. doi:10.1021/es0524301.

Krupa, S.V., Grunhage, L., Jager, H.J., Nosal, M., Manning, W.J., Legge, A.H., Hanewald, K., 2006. Ambient ozone (O_3) and adverse crop response: a unified view of cause and effect. Environmental Pollution 87, 119–126.

Lee, P., Kang, D., McQueen, J., Tsidulko, M., Hart, M., DiMego, G., Seaman, N., Davidson, P., 2008. Impact of domain size on modeled ozone forecast for the Northeastern United States. Journal of Applied Meteorology Climatology 47, 443–461.

Mathur, R., Yu, S., Kang, D., Schere, K.L., 2008. Assessment of the wintertime performance of developmental particulate matter forecasts with the Eta-Community Multiscale Air Quality modeling system. Journal of Geophysical Research-Atmosphere 113 (D02303). doi:10.1029/2007JD008580.

McHenry, J.N., Ryan, W.F., Seaman, N.L., Coats Jr., C.J., Pudykiewicz, S.A., Vukovich, J.M., 2004. A real-time Eulerian photochemical model forecasting system: overview and initial ozone forecast performance in the Northeast U.S. Corridor. Bulletin of the American Meteorological Society (April issue), 525–548.

McKeen, S., Wilczak, J., Grell, G., Djalalova, I., Peckham, S., Hsie, E.-Y., Gong, W., Bouchet, V., Menard, S., Moffet, R., McHenry, J., McQueen, J., Tang, Y., Carmichael, G.R., Pagowski, M., Chan, A., Dye, T., Frost, G., Lee, P., Mathur, R., 2005. Assessment of an ensemble of seven real-time ozone forecasts over eastern North America during the summer of 2004. Journal of Geophysical Research-Atmosphere 110 (D21307). doi:10.1029/2005JD005858.

Mckeen, S., Chung, S.H., Wilczak, J., Grell, G., Djalalova, I., Peckhamm, S., Gong, W., Bouchet, V., Moffet, R., Tang, Y., Carmichael, G.R., Mathur, R., Yu, S., 2007. Evaluation of several $PM_{2.5}$ forecast models using data collected during the ICARTT/NEAQS 2004 field study. Journal of Geophysical Research-Atmosphere 112 (D10S20). doi:10.1029/2006JD007608.

Otte, T.L., Pouliot, G., Pleim, J.E., Young, J.O., Schere, K.L., Wong, D.C., Lee, P.C.S., Tsidulko, M., McQueen, J.T., Davidson, P., Mathur, R., Chuang, H.Y., DiMego, G., Seaman, N.L., 2005. Linking the Eta model with the community multiscale air quality (CMAQ) modeling system to build a national air quality forecasting system. Weather Forecasting 20, 367–384.

Schell, B., Ackermann, I.J., Hass, H., Binkowski, F.S., Ebel, A., 2001. Modeling the formation of secondary organic aerosol within a comprehensive air quality model system. Journal of Geophysical Research-Atmosphere 106, 28275–28293.

Simpson, D., Guenther, A., Hewitt, C.N., Steinbrecher, R., 1995. Biogenic emissions in Europe. 1. Estimates and uncertainties. Journal of Geophysical Research-Atmosphere 100D, 22875–22890.

Tie, X., Brasseur, G., Ying, Z., 2010. Impact of model resolution on chemical ozone formation in Mexico City: application of the WRF-Chem model. Atmospheric Chemistry and Physics 10 (18), 8983–8995.

U.S. EPA, 2010. National ambient air quality standards for ozone, 40 CFR parts 50 and 58, [EPA–HQ–OAR–2005–0172; FRL–9102–1], RIN 2060–AP98. Federal Register 75 (11), 2938–3052. also Available at: http://www.epa.gov/groundlevelozone/fr/20100119.pdf.

Utell, M.J., 2006. Inhalation of ultrafine particles alters blood leukocyte expression of adhesion molecules in humans. Environmental Health Perspectives 114, 51–58.

Yarwood, G., Rao, S., Yocke, M., Whitten, G.Z., 2005. Updates to the Carbon Bond Mechanism: CB05. http://www.camx.com/publ/pdfs/CB05_Final_Report_120805.pdf Report to the U.S. Environmental Protection Agency, December 2005.

Yu, S., Mathur, R., Schere, K., Kang, D., Pleim, J.E., Otte, T.L., 2007. A detailed evaluation of the Eta-CMAQ forecast model performance for O_3, its related precursors, and meteorological parameters during the 2004 ICARTT study. Journal of Geophysical Research-Atmosphere 112 (D12S14). doi:10.1029/2006JD007715.

Yu, S., Mathur, R., Schere, K., Kang, D., Pleim, J.E., Young, J., Tong, D., Pouliot, G., McKeen, S.A., Rao, S.T., 2008. Evaluation of real-time $PM_{2.5}$ forecasts and process analysis for $PM_{2.5}$ formation over the eastern United States using the Eta-CMAQ forecast model during the 2004 ICARTT study. Journal of Geophysical Research-Atmosphere 113 (D06204). doi:10.1029/2007JD009226.

Zhang, Y., Pun, B., Vijayaraghavan, K., Wu, S.-Y., Seigneur, C., Pandis, S., Jacobson, M., Nenes, A., Seinfeld, J.H., 2004. Development and application of the model of aerosol dynamics, reaction, ionization and dissolution (MADRID). Journal of Geophysical Research-Atmosphere 109 (D01202). doi:10.1029/2003JD003501.

Zhang, Y., Huang, J.-P., Henze, D.K., Seinfeld, J.H., 2007. Role of isoprene in secondary organic aerosol formation on a regional scale. Journal of Geophysical Research-Atmosphere 112 (D20207). doi:10.1029/2007JD008675.

Zhang, Y., 2008. Online coupled meteorology and chemistry models: history, current status, and outlook. Atmospheric Chemistry and Physics 8, 2895–2932.

Zhang, Y., Vijayaraghavan, K., Wen, X.-Y., Snell, H.E., Jacobson, M.Z., 2009. Probing into regional O_3 and PM pollution in the U.S., part II. An examination of formation mechanisms through a process analysis technique and sensitivity study. Journal of Geophysical Research-Atmosphere 114 (D22305). doi:10.1029/2009JD011900.

Zhang, Y., Wen, X.-Y., Jang, C.J., 2010a. Simulating climate–chemistry–aerosol–cloud-radiation feedbacks in Continental U.S. using online-coupled WRF/Chem. Atmospheric Environment 44 (29), 3568–3582.

Zhang, Y., Pan, Y., Wang, K., Fast, J.D., Grell, G.A., 2010b. Incorporation of MADRID into WRF/Chem and initial application to the TexAQS-2000 episode. Journal of Geophysical Research-Atmosphere 115 (D18202). doi:10.1029/2009JD013443.

Zhang, Y., Liu, P., Liu, X.-H., Pun, B., Seigneur, C., Jacobson, M.Z., Wang, W.-X., 2010c. Fine scale modeling of wintertime aerosol mass, number, and size distributions in Central California. Journal of Geophysical Research-Atmosphere 115 (D15207). doi:10.1029/2009JD012950.

Zhu, S., Zhang, Y., 2011. Sensitivity of Simulated Chemical Concentrations and Aerosol-Meteorology Interactions to Aerosol Treatments in WRF/Chem, Presentation at the European Geosciences Union General Assembly 2011 and oral presentation at the COST Action ES1004: 'EuMetChem' scientific meeting, Vienna, Austria, April 3–8.